Swimming at Low Reynolds Number: From Sheets to the African Trypanosome

Sujin B. Babu, Christian Schmeltzer, and Holger Stark

Abstract. The African trypanosome is a protozoan which causes sleeping sickness in mammals. To study the dynamics of this microorganism at low Reynolds number, we implement and investigate three swimmer models, the Taylor sheet, a constant-torque swimmer, and a model for the African trypanosome. The first two swimmers are based on a semi-flexible sheet and the third is a full three-dimensional model. We simulate the viscous fluid environment of the swimmers using a technique called multi-particle collision dynamics. We verify our technique by implementing the Taylor sheet which is activated by a bending wave traveling along the sheet. Its ballistic motion turns into diffusive motion when the sheet becomes passive. For the constant-torque swimmer we apply a torque to the semi-flexible sheet which assumes a cork-screw shape and then generates the thrust force for propelling the swimmer forward. Whereas the angular velocity scales linearly with the torque, the swimming velocity displays a non-linear dependence. Finally, our trypanosome model swims with the help of a beating flagellum attached to the cell body. Since it wraps around the body, the model trypanosome displays a helical swimming trajectory. The swimming velocity displays a non-linear increase with the beating frequency of the flagellum.

1 Introduction

The locomotion of microorganisms in viscous environment at low Reynolds number has recently received increasing attention. One reason is the development of new experimental techniques that allow to explicitly study cell motility by using fluorescent staining of bacterial flagella [29], by measuring forces on the single cell level [6],

Sujin B. Babu · Christian Schmeltzer · Holger Stark
Institut für Theoretische Physik, Technische Universität Berlin, Hardenbergstraße 36, D-10623 Berlin, Germany
e-mail: sujin@itp.physik.tu-berlin.de, christian.schmeltzer@gmx.de, holger.stark@tu-berlin.de

C. Tropea and H. Bleckmann (Eds.): Nature-Inspired Fluid Mechanics, NNFM 119, pp. 25–41.
springerlink.com

and by monitoring the kinematics of a cell using optical traps or video microscopy [6]. The physics governing swimming in the microscopic world is completely different from the macroscopic world. On a micron scale inertia is negligible and microorganisms have to resort to a propulsion mechanism where they are constantly in motion in order to translate forward [19, 26]. These propulsion mechanisms are numerous and include the flagellar breast stroke of Chlamydomonas reinhardtii [9] and the planar flagellar beating of sperm cells [5, 28]. In the latter case a wave runs along the flagellum which pushes the sperm cell forward. The propulsion mechanisms are adapted to the environment in which they have to survive.

The goal of the present study is to model the locomotion of the African trypanosome, the microorganism which causes the sleeping sickness, a deadly disease in humans [27]. Trypanosomes are passed into the blood stream of a mammal after a bite from the carrier tsetse fly through its saliva. Their life cycle mainly consists of two stages. First, they reproduce in the carrier's mid gut. Second, they travel through their host's blood vessels and after passing through the blood-brain barrier they cause the deadly disease. The elongated cell body of trypanosomes has the shape of a spindle [see Fig. 1(c)] and the cytoskeleton is made up from microtubules, a very stiff biopolymer with a persistence length of order 1mm [34].

The microtubules start from the thick posterior end and extend along the long axis of the cell body towards the thin anterior end. However, not all microtubules reach the anterior end [27]. In addition, they are linked to each other by proteins. This gives the whole cell body of the African trypanosomes a bending stiffness.

Furthermore, the trypanosome has a single flagellum attached to the cytoskeleton of the cell body. So, as the flagellum beats, the cell body of the trypanosome also bends and twists with the flagellum [11, 29]. The flagellum has the classical 9+2 microtubule axonem as in most eukaryotic cells [4]. The African trypanosome is about $25\mu m$ in length and travels at a speed of $20\mu m/s$ in the highly crowded, viscoelastic blood environment [11]. Experiments have shown that the trypanosome survives in the blood stream since it is able to evade attack from human antibodies by using its motility [11]. So, to prevent this survival strategy, it is very important to fully understand the motility of the trypanosome including the way the flagellum is attached to the cell body and also the flagellar beating pattern. This may help to identify an effective cure for sleeping sickness as the motility of the organism comes only from the flagellum [4].

To study various propulsion mechanism, simplified models have been introduced such as the Taylor sheet [32], the Purcell swimmer [26], and the squirming sphere [8, 20]. They capture the basic physics of the different propulsion mechanisms. In the following, we aim at understanding the locomotion of trypanosomes by first introducing and studying simplified swimmers before we address the complex swimming mode of the African trypanosome. All natural swimmers use drag anisotropy (as explained in Sect. 2.3) to propel themselves through the fluid [19]. In the first artificial swimmer proposed by Taylor in 1951 a sine wave passes along a planar sheet and pushes it forward [32]. We will model it as a semiflexible sheet, which resists

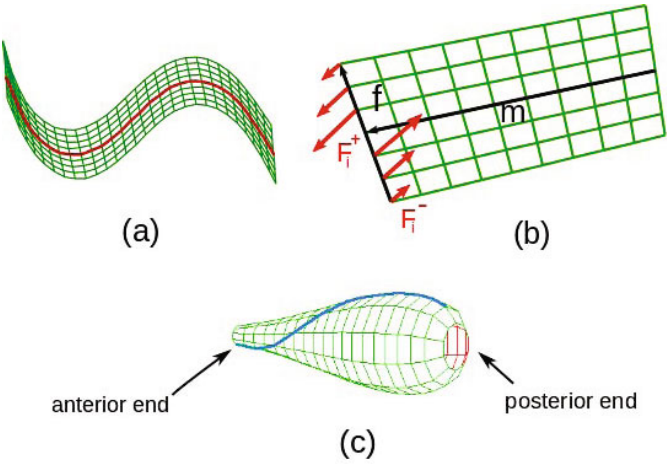

Fig. 1 Illustration of the three swimmers: (a) Undulating Taylor sheet, (b) constant torque swimmer with forces acting along one edge and (c) African trypanosome with the attached flagellum.

bending, and call it the Taylor sheet [see Fig. 1(a)]. In the following, we will explain how we model the sheet, how we actuate it by a sine-wave deformation, and how we couple it to a viscous environment. The moving Taylor sheet initiates flow fields in the fluid, which we simulate with a method called multi-particle collision dynamics (MPCD) [14]. MPCD solves the Navier-Stokes equations using fictitious or coarse grained fluid particles that obey artificial dynamics which locally conserve momentum. Thermal fluctuations are inherent within the technique. MPCD has been widely used to study a variety of problems such as the dynamic properties of semiflexible polymers or sheets [2, 7], single and collective behavior of micro swimmers at low Reynolds number [8, 36], and sedimentation of colloids [24].

In Sect. 2 we explain in detail how we model the swimming Taylor sheet, introduce a second artificial swimmer, which we name constant-torque swimmer, and introduce our model for the African trypanosome based on the semiflexible sheet. Details about our simulation method including a description of MPCD follow. Finally, we finish Sect. 2 with some comments on swimming at low Reynolds number. In Sect. 3 we present our results for the different types of swimmers. In Sect. 3.1 we will show that our modeled Taylor sheet reproduces the swimming behavior as predicted in [32]. In Sect. 3.2 we discuss how angular and linear velocity of the torque swimmer scale with the acting torque. Finally, in Sect. 3.3 we will demonstrate that our model for the African trypanosome captures the essential features seen in experiments. More details of this investigation will be presented in Ref. [3]. We close with conclusions in Sect. 4.

2 Modeling Three Swimmers

In modeling all three swimmers (see Fig. 1) reported in this work, we use a network of vertices connected by springs and with additional bending rigidity to form semiflexible surfaces. Fig. 1(a) illustrates the Taylor sheet [32], where a sine wave propagates along a semiflexible plane surface. It pushes the sheet forward similar to the flagellar beat of a sperm cell. In the constant-torque swimmer of Fig. 1(b) a torque is applied to one edge of a semiflexible sheet. It deforms to a screw-like object which creates a thrust force that propels the swimmer. Finally, Fig. 1(c) shows the complete three-dimensional model of the African trypanosome where the blue line represents the flagellum attached to the cell body. When a wave passes along the flagellum, the whole cell body distorts. Now, we introduce the modeling of each swimmer in the following subsections.

2.1 Taylor Sheet

In Ref. [2] we have explained in detail how we model a semiflexible sheet in three dimensions, when we studied its thermal motion in a viscous fluid. Here we just mention the key features. The vertices of the sheet are distributed on a square lattice. Adjacent vertices with equilibrium distance l_0 are connected by Hookean springs with the potential energy

$$U_s = \frac{1}{2}\kappa_s (l - l_0)^2, \tag{1}$$

where l is the actual distance. In order to prevent the sheet from shearing, next-nearest neighbor vertices along the diagonal of the square unit cell are also connected by springs. In order to prevent the sheet from crumpling, we also apply a bending potential along the two main directions of the sheet,

$$U_b = \kappa_b (1 - \cos\theta). \tag{2}$$

Here κ_b is the bending stiffness and θ is the angle between two bond vectors that point from one vertex to its two nearest neighbors [13].

To propel the sheet, we apply a bending wave along the center line of the sheet using the potential

$$U_w = \kappa_w (1 - \cos[\mathbf{t}_{i+1} \cdot \mathbf{R}(\alpha_\mathrm{w})\mathbf{t}_i]) \quad \text{with} \quad \alpha_\mathrm{w} = A \sin(kd_i - \omega_\mathrm{w} t). \tag{3}$$

Here κ_w is again some bending stiffness with respect to a bent reference state. To introduce this state, we rotate one tangent or bond vector of the sheet, $\mathbf{t}_i$, against the neighboring bond vector $\mathbf{t}_{i+1}$ using the rotation matrix $\mathbf{R}(\alpha_\mathrm{w})$, where $|\mathbf{t}_i| = |\mathbf{t}_{i+1}| = 1$. The matrix $\mathbf{R}(\alpha_\mathrm{w})$ rotates $\mathbf{t}_i$ by an angle α_w about the direction perpendicular to the center line and tangential to the sheet. Now, the rotation angle α_w varies like a

propagating sine wave along the center line with amplitude A, which is always one in all our simulations. Further characteristics of the wave are the wave number $k = \frac{2\pi}{\lambda}$, where λ is the wavelength, and the angular frequency ω_w. Time t is measured in the time unit of the MPCD method and d_i is the distance from one end of the sheet to the vertex i on the centerline of the sheet.

2.2 Constant-Torque Swimmer

The second swimmer reported here is a semiflexible sheet which we set in rotation with the help of an external torque. In practice, we apply forces on the vertices along one edge of the sheet as illustrated in Fig. 1 (b). The total torque $\mathbf{M}$ becomes

$$\mathbf{M} = \kappa_t \sum_i \mathbf{r}_i \times \mathbf{F}_i. \tag{4}$$

Here $\mathbf{r}_i$ points from the centerline to one vertex. We introduce a unit vector $\mathbf{t}$ as tangent to the centerline and define the vector $\mathbf{F}_i = \mathbf{r}_i \times \mathbf{t}/r_i^2$ such that each vertex contributes the same torque κ_t. Thereby we keep the edge of the sheet straight. The forces from both sides of the centerline cancel each other so that the total force on the sheet is zero. Since the sheet is semiflexible, it assumes the shape of a corkscrew when it rotates. Thereby a thrust force is generated which pushes the swimmer forward.

2.3 African Trypanosome

In Fig. 1(c) we show our model surface for the African trypanosome which we used in the simulations. The diameters for the different cross sections of the cell body vary according to

$$S(i) = (i+0.15)^{1/4} \exp[-0.006(i+0.15)^2] \ , \ 0 \leq \mathrm{i} < 20. \tag{5}$$

The diameters are given in units of l_0 and i is the index of the cross section starting with 0 at the thicker posterior end. The function $S(i)$ was constructed such that it reproduces the characteristic shape of the trypanosome. On each circle with diameter $S(i)$ 10 vertices are equally distributed so that they define a dodecagon. All vertices shown in Fig. 1(c) are connected by Hookean springs using the spring potential of Eq. (1). In addition, internal springs connect opposite vertices of the cross-sectional dodecagon. This helps to keep the shape and thereby the volume of the cell body. We chose relatively high values for the spring constant ($\kappa_s = 10^7$) which means very stiff springs.

To mimic the microtubules which run along the long axis of the cell body, we apply a bending potential along each line of vertices from the posterior to the anterior end:

$$U_b = \frac{1}{2}\kappa_b(\cos\theta_0 - \cos\theta)^2. \tag{6}$$

Here θ is the angle between two adjacent bond vectors and θ_0 is the equilibrium angle according to the equilibrium shape of the cell body given by Eq. (5). The bending stiffness κ_b allows for deformations of the cell body. In real African trypanosomes not all microtubules reach the anterior end, so this end is more flexible than the posterior end. To simulate this effect, we progressively reduce the bending stiffness by a factor of 0.95 starting from the center of the cell body so that the bending stiffness at the anterior end is given by $(0.95)^{10}\kappa_b = 0.60\kappa_b$. Reducing this factor further destabilizes the model cell body. In the simulations both the anterior and posterior end are closed by hemispheres. They are not visible in Fig. 1(c). The length-to-thickness ratio of the African trypanosome is around 8, in our modeling we always keep this value at approximately 7.5 thereby being as close as possible to the real cell body.

We define the flagellum using the vertices of the cell body. So the model flagellum is by definition firmly attached to the cell body and thereby mimics the real trypanosome. There is a current debate how the flagellum runs along the cell body: Is it straight or does it wrap about the cell body [29]. Following observations from our experimental colleagues [10], the flagellum is straight starting from the thick posterior end till the center of the cell body and then wraps in a half turn around the cell body as shown by the blue line in Fig. 1(c). Along this flagellum, we pass a planar bending wave with the help of the potential given in Eq. (3). The only difference is that the matrix $\mathbf{R}(\alpha_{\mathrm{w}})$ refers to a rotation about the local normal of the cell body. Experiments have demonstrated that the end-to-end distance of the cell body of a swimming trypanosome amounts to ca. 60% of its cell body length [33]. We have adjusted the values of the parameters κ_s, κ_b and κ_w such that in the simulations the end-to-end distance is around 76%. A further reduction destabilizes the cell body.

2.4 Dynamics of the Swimmers

Vertices that define the surfaces of our swimmers experience forces through the spring and bending potentials. We assign to each vertex a mass $m = 1$ (in MPCD units introduced below) and move it by a typical molecular dynamics step. Positions and velocities are updated using the velocity Verlet algorithm [1] where δt_{MD} is the integration time step:

$$\mathbf{r}_i(t+\delta t_{MD}) = \mathbf{r}_i(t) + \delta t_{MD}\mathbf{v}_i(t) + \frac{1}{2}\delta t_{MD}^2 \frac{\mathbf{F}_i(t)}{m} \tag{7}$$

$$\mathbf{v}_i(t+\delta t_{MD}) = \mathbf{v}_i(t) + \frac{1}{2}\delta t_{MD}\left[\frac{\mathbf{F}_i(t)}{m} + \frac{\mathbf{F}_i(t+\delta t_{MD})}{m}\right]. \tag{8}$$

Here $\mathbf{r}_i$ and $\mathbf{v}_i$ are the respective position and velocity of the ith vertex of the cell body and $\mathbf{F}_i = -\nabla_i(U_s + U_b + U_w)$ is the force acting on this vertex. To perform the gradient ∇_i of the spring, bending, and bending wave potentials $U_s + U_b + U_w$ with respect to $\mathbf{r}_i$, the energies are discretized in the position variables $\mathbf{r}_i$. To keep the cell body stable, we always chose $\delta t_{MD} \ll 1$ in all the simulations reported here. While

both the total force and torque acting on the Taylor sheet and the model trypanosome are zero, only the total force on the constant-torque swimmer vanishes.

The swimmers also experience frictional forces from their viscous environment. We now describe how we model the fluid flow created by the swimmers when they move around.

2.5 Modeling the Newtonian Fluid

We determine the flow field around the swimmers with a method called multi-particle collision dynamics (MPCD). This method introduces coarse-grained or fictitious fluid particles that obey an artificial dynamics through a succession of ballistic and collision steps. The important point is that during the collision step momentum is conserved. So, on sufficiently long time and length scales, the MPCD method is equivalent to solving the Navier-Stokes equations [21, 22]. For the MPCD algorithm one can also derive analytic expressions for the fluid viscosity and thereby control it easily. At low Reynolds number, where one has to solve Stokes equations, MPCD is a quick simulation technique and relatively easy to implement [14]. In addition, MPCD includes thermal fluctuations. After some equilibration, the velocities of the fluid particles are Gaussian distributed with a variance of $3k_BT/m$ around a mean value as expected for a fluid in local thermal equilibrium.

We start the simulations by placing point particles in a simulation box with linear dimension L_{box}. To reduce the equilibration time, we already assign to each of the fluid particles a velocity from a Gaussian distribution with variance $3k_BT/m$, where k_B is the Boltzmann constant, T is temperature, and m is the mass of the fluid particle. In MPCD units, we set thermal energy $k_BT = 1$ and $m = 1$. Now, MPCD launches a two-step dynamics consisting of the streaming and collision step. In the streaming step the fluid particles move ballistically during a small time intervall δt:

$$\mathbf{r}_i(t+\delta t) = \mathbf{r}_i(t) + \delta t \mathbf{v}_i(t) \quad . \tag{9}$$

Here $\mathbf{r}_i(t)$ and $\mathbf{r}_i(t+\delta t)$ are the respective positions of the particle i before and after the streaming step and $\mathbf{v}_i(t)$ is its velocity. In the collision step we divide our simulation box into cells with linear dimension $a = 1$. The density of the fluid particles ρ_0 is kept at 10, which means, on average, 10 particles per cell. We now follow a procedure known from the Anderson thermostat in a conventional molecular dynamics simulation [14]. We calculate the center of mass velocity of each cell, $\mathbf{V}(t)$, and then assign to each particle in the cell a random relative velocity $\mathbf{v}_{i,ran}$ from a Gaussian distribution with variance $3k_BT/m$:

$$\begin{aligned} \mathbf{v}_i^{\text{new}}(t) = \mathbf{V}(t) + \mathbf{v}_{i,ran} - \sum_{cell} \mathbf{v}_{i,ran}/N_c \\ + m\Pi^{-1} \sum_{j \in cell} \left[\mathbf{r}_{j,c} \times (\mathbf{v}_j - \mathbf{v}_j^{ran})\right] \times \mathbf{r}_{i,c}. \end{aligned} \tag{10}$$

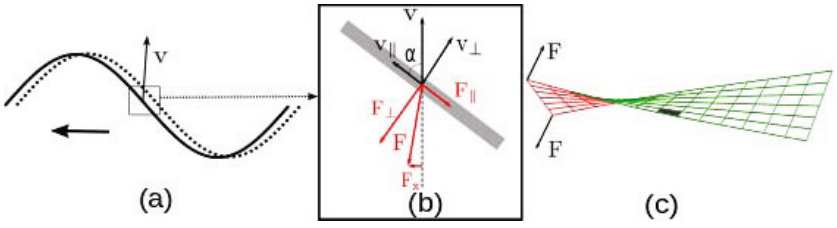

Fig. 2 (a) A bending wave propagates along a filament to the right which pushes the filament to the left indicated by thick black arrow. (b) Blow up of a local segment of the filament. Anisotropic friction produces a thrust force to the left. (c) Rotating segment of the constant torque swimmer also produce a thrust force.

The third term on the right-hand side is added to conserve the center of mass velocity or momentum during collision in the cell. The last term in Eq. (10) implements angular momentum conservation. For example, in our system where the trypanosome also rotates in space, it is important to avoid unphysical behavior. The advantage of using the idea of the Anderson thermostat for the collision step is also that temperature is, by definition, kept constant. Finally, we shift the simulation grid randomly before each collision step, in order to avoid unphysical correlations between the particle velocities and thereby restore Galilean invariance [16, 17].

To couple our swimmers to the MPCD fluid, we include their vertices in the collision step. In addition, for the model trypanosome the fluid particles are not allowed to go through the cell body by applying a stochastic bounce back rule [23, 25], which implements the no-slip boundary condition at the surface. However, for our sheet swimmers, we let the fluid particles move through the sheet during the streaming step. In Ref. [2] we showed that this procedure does not change the dynamics of the sheets but saves considerable simulation time. The reason is the following. Both, collision and streaming steps contribute to the viscosity of the MPCD fluid [14]. However, in particular at low Reynolds number the collision step mainly determines viscosity and the transfer of momentum between the fluid particle and the vertices mainly comes from the collision step. So details of the streaming step are not important.

2.6 Swimming at Low Reynolds Number

The African trypanosome has a typical length of $L \approx 25\mu m$ and swims in water with a velocity of about $v \approx 5\mu m$. This results in a Reynolds number $\mathrm{Re} = Lv\rho/\eta \approx 10^{-4}$ where η is the viscosity of water and ρ its density. So inertia does not play any role and fluid flow is governed by the Stokes equations, which result from the Navier-Stokes equations by setting the inertial term to zero. Microorganisms swimming in this world of low Reynolds number cannot drift by inertia [31]. When they stop with their actuation mechanism they almost immediately stop moving forward. In other words, the momentum of the swimmer is dissipated into the fluid instantaneously

which is called overdamped limit. A passive body only moves when an external force is applied and its velocity is proportional to this force. This is the signature of Aristotelian mechanics.

The Stokes equations, $\mathbf{0} = -\nabla p + \eta \nabla^2 \mathbf{u}$, where p is pressure and $\mathbf{u}$ is the velocity field, allow for time-reversed solutions, when also pressure forces and external forces are reversed. This kinematic reversibility has important consequences. A potential swimmer cannot move forward with a reciprocal actuation cycle, meaning a cycle which looks the same under time reversal. This is the content of Purcell's famous scallop theorem [26]. Swimming at low Reynolds number needs a non-reciprocal actuation cycle.

Figure 2(a) shows a wave traveling along a filament at two instances of time. Obviously, the motion is non-reciprocal. The local segment has to move upwards to realize the filament at a later time. A thrust force that pushes the filament forward [see Fig. 2(b)] can only exist since the friction coefficients for moving the segment parallel ($\xi_\parallel$) or perpendicular ($\xi_\perp$) to its axis differ. In fact, $\xi_\parallel = F_\parallel / v_\parallel < \xi_\perp = F_\perp / v_\perp$, which explains the thrust force F_x in Fig. 2(b). Calculating F_x results in

$$F_x = \left(\xi_\parallel - \xi_\perp\right) v \sin\alpha \cos\alpha. \tag{11}$$

In principle, all three swimmers use anisotropic friction coefficients to generate their thrust force. The Taylor sheet is just the waving filament extended into the second dimension. Rotating the constant-torque swimmer [see Fig. 2(c)], one locally has the situation as in Fig. 2(b), in principle. Finally, the whole body of the African trypanosomes performs a wave-like motion initiated by the attached flagellum.

3 Results

We now present our simulation results for the three swimmers introduced in the previous section.

3.1 Taylor Sheet

As explained in Sect. 2.1, we apply a sine bending wave along the centerline of the semiflexible sheet. In Fig. 3 we plot a snapshot of the sheet and the trajectory of one of its vertices. The whole sheet takes over the bending wave of the centerline and travels in opposite direction to the wave propagation as explained in Sect. 2.6. [32]. Since our sheet is essentially inextensible, each vertex moves along a figure 8 instead of just oscillating up and down as suggested in Fig. 2(b).

The mean-square displacement (MSD) for the center of mass of the sheet is defined as

$$\langle R^2 \rangle = \langle [\mathbf{r}_{cm}(t) - \mathbf{r}_{cm}(0)]^2 \rangle, \tag{12}$$

where $\mathbf{r}_{cm}$ denotes the position of the center of mass. As long as the sheet is propelled by the bending wave, it moves ballistically as indicated in Fig. 4, where

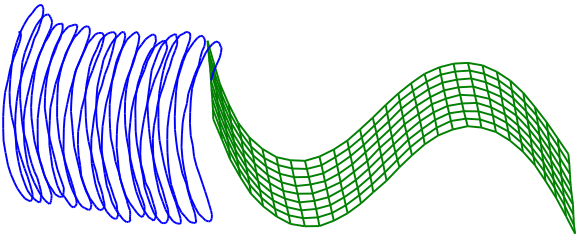

Fig. 3 Snapshot of the Taylor sheet moving to the right while the bending wave propagates to the left. The trajectory of one vertex is plotted.

$\langle R^2 \rangle \propto t^2$. When we stop the actuation of the sheet, the sheet behaves as a passive object or Brownian particle with the typical diffusive behavior, $\langle R^2 \rangle \propto t$, as demonstrated in Fig. 4 and in agreement with our earlier work [2].

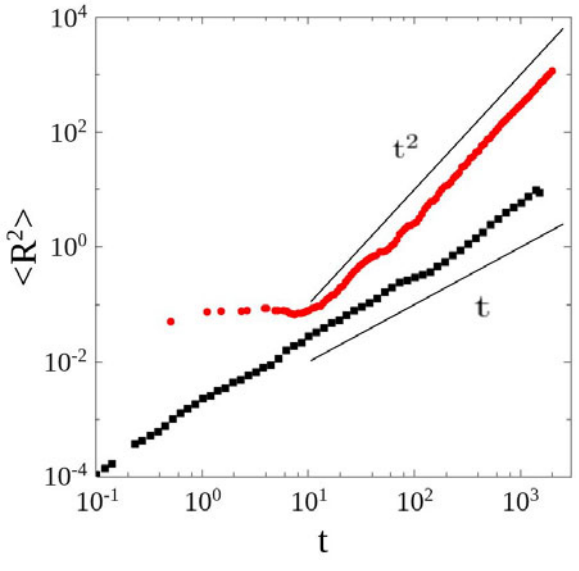

Fig. 4 MSD of the center of mass for the Taylor sheet swimmer (red) and a passive semiflexible sheet (black). The ballistic and diffusive motion are indicated, respectively, by the power laws $\propto t^2$ and $\propto t$.

3.2 Constant-Torque Swimmer

As explained in Sect. 2.2, we apply a torque to a semiflexible sheet parallel to its long axis and very similar to the flexible polymer swimmer of Ref. [12] where the

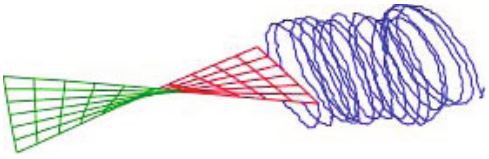

Fig. 5 The constant-torque swimmer assumes the shape of a cork screw when it rotates due to an applied torque. The rotation generates a thrust force and moves parallel to the applied torque as indicated by the trajectory of one vertex.

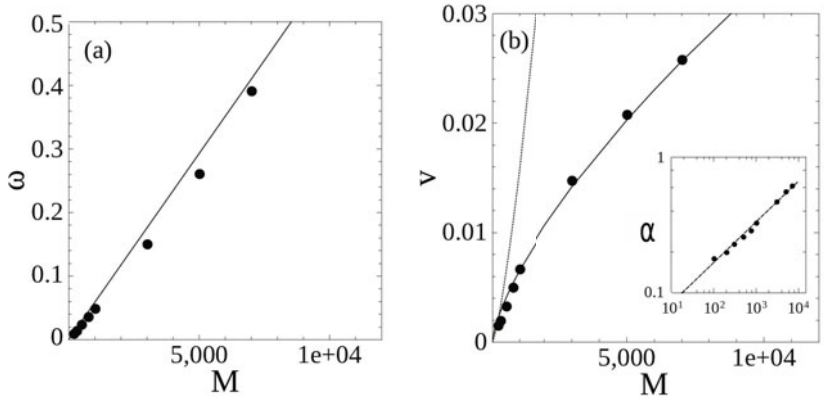

Fig. 6 (a) Angular velocity ω versus driving torque M in MPCD units. Dots indicate results from the MPCD simulations and the solid line is $\omega = M/\xi_r$. (b) Translational velocity versus driving torque M in MPCD units. Dotted line: Scaling law $v \propto M^{1.3}$ valid for small torques. Full line: Scaling law $v \propto M^{0.7}$ valid for large torques. Inset: Pitch angle α versus torque M. The dashed line is a fit to $\alpha \propto M^{0.3}$.

torque is realized by a rotating magnetic field. Depending on the magnitude of the bending stiffness and the torque, the sheet assumes the shape of a cork screw, as illustrated in Fig. 5 for a sheet of length $L_l = 13$ and width $L_b = 6$. In Sect. 2.6 we just described how the rotation then generates the thrust forces which pushes the screw forward. As a result, the constant-torque swimmer moves parallel to the torque axis. The screw-like motion is indicated by the trajectory of one vertex.

In Fig. 6(a) we plot the angular velocity ω as a function of the applied torque. It increases nearly linearly with the torque. Deviations result from the screw deformation which becomes more pronounced for larger torques. The rotational friction coefficient for a square sheet is isotropic, similar to that of a disc [15], and we determined it with MPCD simulations as $\xi_r = 20\eta L^3$ [30]. As an estimate for our elongated sheet, we use the same formula but replace L by $L = \sqrt[3]{L_l L_b^2}$. Note that $\pi(L_b/2)^2 L_l$ is the cylindrical volume covered by the sheet during a 2π rotation. The

solid line in Fig. 6(a) is just the linear relation $\omega = M/\xi_r$ and good fit to the results from our simulations.

In Fig. 6(b) we plot the translational velocity v versus the applied torque. The dependence is clearly non-linear due to the fact that the sheet deforms into a helical structure with pitch angle α which is defined in Fig. 2(c). The deformation of the sheet into the cork screw structure increases with M which we demonstrate by the inset of Fig. 6(b) for the torque dependence of the pitch angle α. We find that $\alpha \propto M^{0.3}$. For a helical structure translation and rotation are coupled and the following linear relations for force F and torque M acting on the helical structure exist: $F = Av + B\omega$ and $M = Bv + C\omega$. In particular, the non-zero coupling coefficient B produces linear motion from an applied torque. In our case, the applied force F is zero. Eliminating ω with both equations results in the velocity-torque dependence

$$v = \frac{B}{B^2 + AC} M \tag{13}$$

For a helical filament, $B \propto \alpha$ for small pitch angle α [19, 35] and we expect the same to be valid for a twisted sheet. With $\alpha \propto M^{0.3}$ we therefore obtain $B \propto M^{0.3}$. For sufficiently small M or $B^2 \ll AC$ in Eq. (13), we arrive at $v \propto M^{1.3}$ which we fitted with an appropriate prefactor in Fig. 6(b) by the dotted line. Clearly, the scaling law is only valid for the smallest values of M. In our simulations it is difficult to access the regime as it needs a lot of simulation time. On the other hand, for large torques such that $B^2 \gg AC$, one arrives at $v \propto M/B \propto M^{0.7}$ which results in a good fit as the solid line in Fig. 6(b) shows.

3.3 Swimming of the Model African Trypanosome

With the results from the sheet swimmers in mind, we have established a three-dimensional model for the African trypanosome. As explained in Sect. 2.3, a planar sine bending wave passes along the flagellum and tangential to the cell body of the model trypanosome [Fig. 1(c)]. Figure 7(a) shows a snapshot of the swimming trypanosome model. The sine wave propagates from the thin anterior end to the

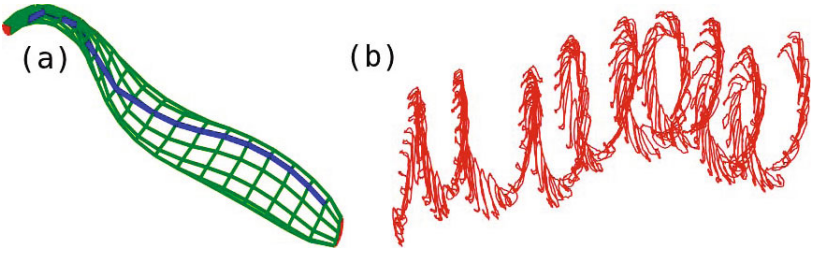

Fig. 7 Snapshot of the African trypanosome during swimming in the MPCD fluid. (b) Helical trajectory of the posterior end of the African trypanosome model simulated for a long time such that helical motion becomes visible.

thick posterior end and pushes the African trypanosome in the opposite direction as explained is Sect. 2.6. In Fig. 7(b) we show the trajectory of one of the vertices at the posterior end. As the bending wave passes through the flagellum, the posterior end moves back and forth on the time scale of the period of the bending wave. For long times the trypanosome moves on a helical trajectory since the flagellum wraps around the cell body. We have followed here new experimental results [10]. In these experiments, the trypanosome needs eight beating cycles of its flagellum to perform a full 2π rotation. In contrast, our model needs 23 beating cycles.

The real swimming trypanosome has an average end-to-end distance $\overline{\varepsilon}$ of about 60% of its cell length [33]. In Fig. 8(a) we plot the time dependence of ε for our model trypanosome during swimming which is similar to experiments [33]. However, $\varepsilon(t)$ varies between 0.7 and 0.85 with an average of about 0.76 which is above the experimental value. Our attempts to reduce this value failed since the model trypanosome became unstable. We also performed relaxation experiments reported elsewhere where we let the model trypanosome relax under a steady bending wave [3]. Typically, the relaxation time is smaller than the period of the beating flagellum in a swimming trypanosome.The model trypanosome thus goes through quasi-equilibrium states such that its shape is always fully relaxed. We have indications that the real trypanosome swims in the same regime [3].

Figure 8(b) plots the velocity as a function of the angular frequency on a double logarithmic scale for 2 different viscosities in MPCD units. The velocity increases with frequency following the scaling law $v \propto \omega_w^{1/2}$ as indicated by the line. In contrast, for the Taylor sheet or the beating flagellum one expects a linear relationship [32]. The main reason is that the beating flagellum of the trypanosome has to move a large cell body with a large friction coefficient. Using an idea of Lauga [18] we are able to deduce the $\omega_w^{1/2}$ scaling law [3]. Deviations from it are visible in

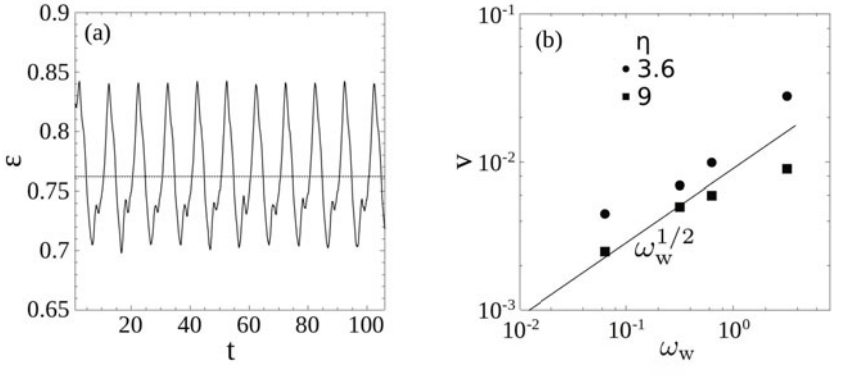

Fig. 8 (a) End-to-end distance ε of the swimming model trypanosome (in units of the body length) as a function of time. The dashed line is $\overline{\varepsilon} = 0.76$. (b) Swimming velocity v versus beating frequency ω_w of the flagellum for two different viscosities η in MPCD units.

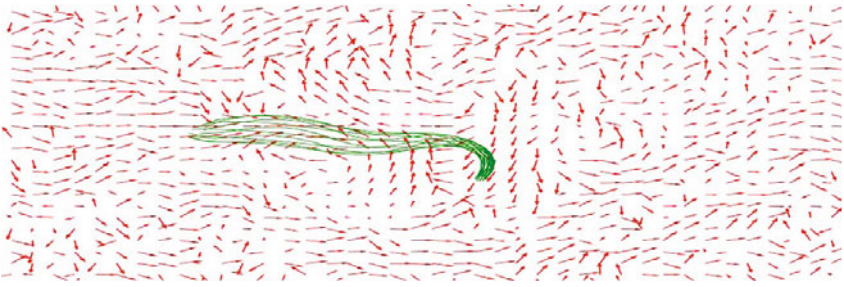

Fig. 9 The average flow field as obtained from simulations. The cell body is shown as guide to the eye.

Fig. 8(b) at the larger viscosity and for large ω. Larger viscosity means that the relaxation time under a static bending wave increases. So beyond $\omega_w = 1$, our model trypanosome does not pass anymore through quasi-equilibrium states. Clearly, increasing viscosity results in a decrease of the swimming speed since the drag force on the cell body increases. Ultimately, for very long time the model trypanosome will change its direction due to rotational diffusion of the cell body and will perform a random walk similar to the real trypanosome [37]. However, in our simulations rotational diffusion would be only of thermal origin whereas in the real trypanosome intrinsic noise enhances the rotational diffusion constant [37].

From MPCD simulations we also obtain the flow field of the fluid around the moving trypanosome. In Fig. 3.3 we plot the flow field in the plane which contains the trypanosome. The plot is an average over the calculated flow fields for several 2π rotations of the trypanosome. For clarity, all velocities have the same strength and we show one snapshot of the model trypanosome. We observe that close to the cell body there is flow from the thin anterior end towards the thick posterior end and also flow from the posterior end towards the swimming direction. A small particle close to the anterior end is propelled by the flow field towards the posterior end where the flagellum pocket is situated. Experiments showed that antibodies from the host are dragged along the surface of the cell body towards the flagellum pocket where they are internalized into the cell body [11]. The trypanosome uses such a strategy to defend itself against antibodies. The flow field from our simulations, at least, qualitatively confirms the strategy. It also gives us confidence that our simulations with the model trypanosome generate a swimming behavior very close to the real organism.

4 Conclusion

In this article we introduced and investigated three swimmer models with the help of the particle based MPCD method which allows to calculate flow fields in arbitrary geometries. The Taylor sheet is a semi-flexible sheet propelled by a bending wave along its center line. Whereas the active sheet moves ballistically, the passive sheet

displays conventional diffusive behavior in agreement with our earlier work [2]. The constant-torque swimmer is set into rotation by forces along one of its edges. It deforms into a cork screw through the friction with the surrounding fluid and thereby creates a thrust force that pushes the swimmer forward. The angular velocity is nearly linear in the applied torque M. The translational velocity displays a non-linear dependence on M due to the changing pitch angle of the cork screw. The frictional coupling coefficient directly depends on this pitch angle. After having implemented semi-flexible sheet structures, we were able to introduce a three-dimensional model for the African trypanosome and to couple it to the MPCD fluid. The bending wave passing along the attached flagellum from the thin anterior to the thick posterior end propels the trypanosome towards the anterior end while the trypanosome rotates due to the helical attachment of the flagellum. We obtain oscillations in the end-to-end distance of the cell body as observed in experiments. The translational velocity scales as $\omega_w^{1/2}$, where ω_w is the angular frequency of the bending wave. In Ref. [3] we have developed an understanding for this scaling.

With such a realistic model for the African trypanosome at hand, we are able to study its swimming in microchannels which mimic blood vessels. We will also introduce simple red-blood cells into the MPCD fluid to obtain a more realistic model for blood and investigate why these obstacles under certain conditions improve the swimming of the African trypanosome. So our modeling helps to explore the swimming of the African trypanosome in realistic environments and thereby contributes to its understanding.

Acknowledgements. We like to thank Engstler M, Pfohl T, Kruger T, Uppaluri S and Stellamanns E for helpful discussions. This work has been supported by DFG under grants STA 352/7-2 and STA 352/9-1.

References

1. Allen, M.P., Tildesley, D.J.: Computer Simulation of Liquids. Clarendon, Oxford (1991)
2. Babu, S.B., Stark, H.: Dynamics of semi-flexible tethered sheet. Eur. Phys. J. E 34, 136–142 (2011), doi:10.1140/epje/i2011-11136-2
3. Babu, S.B., Stark, H.: (in preparation, 2012)
4. Broadhead, R., Dawe, H.R., Farr, H., et al.: Flagellar motility is required for the viability of the bloodstream trypanosome. Nature 440, 224–227 (2006), doi:http://dx.doi.org/10.1038/nature04541
5. Camalet, S., Julicher, F.: Generic aspects of axonemal beating. New J. Phys. 2, 24.1–24.23 (2000), doi:10.1088/1367-2630/2/1/3240
6. Chattopadhyay, S., Moldovan, R., Yeung, C., et al.: Swimming efficiency of bacterium Escherichiacoli. Proc. Nat. Acad. Sci. 103, 13712–13717 (2006), doi:10.1073/pnas.0602043103
7. Chelakkot, R., Winkler, R.G., Gompper, G.: Semiflexible polymer conformation, distribution and migration in microcapillary flows. J. Phys. Condens. Matter 23, 184117(1-13) (2011), doi:10.1088/0953-8984/23/18/184117

8. Downton, M.T., Stark, H.: Simulation of a model microswimmer. J. Phys. Condens. Matter 21, 204101(1-6) (2009), doi:10.1088/0953-8984/21/20/204101
9. Drescher, K., Goldstein, R.E., Michel, N., et al.: Direct Measurement of the Flow Field around Swimming Microorganisms. Phys. Rev. Lett. 105, 168101(1-4) (2010), doi:10.1103/PhysRevLett.105.168101
10. Engstler, M., Heddergott, N., Kruger, et al.: African trypanosome as model system for functional analyses of microbial motility. NNFM 119, 43–61 (2012)
11. Engstler, M., Pfohl, T., Herminghaus, S., et al.: Hydrodynamic Flow-Mediated Protein Sorting on the Cell Surface of Trypanosomes. Cell 131, 505–515 (2007), doi:10.1016/j.cell.2007.08.046
12. Garstecki, P., Tierno, P., Weibel, D.B., et al.: Propulsion of flexible polymer structures in a rotating magnetic field. J. Phys. Condens. Matter 21, 204110(1-8) (2009), doi:10.1088/0953-8984/21/20/204110
13. Gauger, E.M., Stark, H.: Numerical study of a microscopic artificial swimmer. Phys. Rev. E 74, 021907(1-10) (2006), doi:10.1103/PhysRevE.74.021907
14. Gompper, G., Ihle, T., Kroll, D.M., et al.: Multi-Particle Collision Dynamics: A Particle-Based Mesoscale Simulation Approach to the Hydrodynamics of Complex Fluids. Adv. Polym. Sci. 221, 1–87 (2009), doi:10.1007/978-3-540-87706-6_1
15. Happel, J., Brenner, H.: Low Reynolds number hydrodynamics: with special application to particulate media. Kluwer, Hauge (1983)
16. Ihle, T., Kroll, D.M.: Stochastic rotation dynamics: A Galilean-invariant mesoscopic model for fluid flow. Phys. Rev. E 63, 020201(1-4) (2001), doi:10.1103/PhysRevE.63.020201
17. Ihle, T., Kroll, D.M.: Stochastic rotation dynamics. I. Formalism, Galilean invariance, and Green-Kubo relations. Phys. Rev. E 67, 066705(1-11) (2003), doi:10.1103/PhysRevE.67.066705
18. Lauga, E.: Floppy swimming: Viscous locomotion of actuated elastica. Phys. Rev. E 75, 041916(1-16) (2007), doi:10.1103/PhysRevE.75.041916
19. Lauga, E., Powers, T.R.: The hydrodynamics of swimming microorganisms. Rep. Prog. Phys. 72, 096601(1-36) (2009), doi:10.1088/0034-4885/72/9/096601
20. Lighthill, M.J.: On the squirming motion of nearly spherical deformable bodies through liquids at very small reynolds numbers. Commun. Pure Appl. Math. 5, 109–118 (1952), doi:10.1002/cpa.3160050201
21. Malevanets, A., Kapral, R.: Mesoscopic model for solvent dynamics. J. Chem. Phys. 110, 8605–8613 (1999), doi:10.1063/1.478857
22. Malevanets, A., Kapral, R.: Solute molecular dynamics in a mesoscale solvent. J. Chem. Phys. 112, 7260–7269 (2000), doi:10.1063/1.481289
23. Padding, J.T., Louis, A.A.: Hydrodynamic interactions and Brownian forces in colloidal suspensions: Coarse-graining over time and length scales. Phys. Rev. E 74, 031402(1-29) (2006), doi:10.1103/PhysRevE.74.031402
24. Padding, J.T., Louis, A.A.: Interplay between hydrodynamic and Brownian fluctuations in sedimenting colloidal suspensions. Phys. Rev. E 77, 011402(1-11) (2008), doi:10.1103/PhysRevE.77.011402
25. Padding, J.T., Wysocki, A., Lowen, H., et al.: Stick boundary conditions and rotational velocity auto-correlation functions for colloidal particles in a coarse-grained representation of the solvent. J. Phys. Condens. Matter 17, S3393–S3399 (2005), doi:10.1088/0953-8984/17/45/027
26. Purcell, E.M.: Life at low Reynolds number. Am. J. Phys. 45, 3–11 (1977), doi:10.1119/1.10903

27. Ralston, K.S., Kabututu, Z.P., Melehani, J.H., et al.: The Trypanosoma brucei Flagellum: Moving Parasites in New Directions. Ann. Rev. Microbio. 63, 335–362 (2009), doi:10.1146/annurev.micro.091208.073353
28. Riedel Kruse, I.H., Hilfinger, A., Howard, J., et al.: How molecular motors shape the flagellar beat. HFSP J. 1, 192–208 (2007), doi:10.2976/1.2773861
29. Rodriguez, J.A., Lopez, M.A., Thayer, C.M., et al.: Propulsion of African trypanosomes is driven by bihelical waves with alternating chirality separated by kinks. Proc. Nat. Acad. Sci. 106, 19322–19327 (2009), doi:10.1073/pnas.0907001106
30. Schmeltzer, C.: unpublished work
31. Strak, H.: Immer in Bewegung Bleiben. Physik. Journal 6(11), 31–37 (2007)
32. Taylor, G.: Analysis of the Swimming of Microscopic Organisms. Proc. R Soc. A 209, 447–461 (1951), doi:10.1098/rspa.1951.0218
33. Uppaluri, S., Nagler, J., Stellamanns, E., et al.: Impact of Microscopic Motility on the Swimming Behavior of Parasites: Straighter Trypanosomes are More Directional. PLoS Comput. Biol. 7, e1002058(1-8) (2011), doi:10.1371/journal.pcbi.1002058
34. Van den Heuvel, M.G.L., de Graaff, M.P., Dekker, C.: Microtubule curvatures under perpendicular electric forces reveal a low persistence length. Proc. Nat. Acad. Sci. 105, 7941–7946 (2008), doi:10.1073/pnas.0704169105
35. Vogel, R., Stark, H.: Submitted to Eur. Phys. J. E (2012)
36. Yang, Y., Elgeti, J., Gompper, G.: Cooperation of sperm in two dimensions: Synchronization, attraction, and aggregation through hydrodynamic interactions. Phys. Rev. E 78, 061903(1-9) (2008), doi:10.1103/PhysRevE.78.061903
37. Zaburdaev, V., Uppaluri, S., Pfohl, T., et al.: Langevin Dynamics Deciphers the Motility Pattern of Swimming Parasites. Phys. Rev. Lett. 106, 208103(1-4) (2011), doi:10.1103/PhysRevLett.106.208103